PERGAMON

International Journal of Heat and Mass Transfer 42 (1999) 3659–3672

International Journal of HEAT and MASS TRANSFER

www.elsevier.com/locate/ijhmt

An experimental investigation of the melting process in a rectangular enclosure

Y. Wang, A. Amiri, K. Vafai*

Department of Mechanical Engineering, The Ohio State University, Columbus, OH 43210, USA

Received 8 September 1998; received in revised form 5 December 1998

Abstract

An experimental investigation of the melting process in the vicinity of a heated vertical wall in a rectangular enclosure is presented in this work. A flat-plate heat pipe was used to provide a uniform temperature source. The liquid flow patterns during the melting process were captured and the instantaneous marching of the liquid–solid interface was presented. In addition, the temperature distributions in the phase change material were measured at the mid-plane as well as top and bottom walls of the enclosure. Three different heat transfer regimes were identified during the melting process. The parametric domain covered the range of $Ra = 2.02 \times 10^6$–2.61×10^7, $Ste\ Fo = 0.001$–0.125 and $Pr = 804$–1055 while the critical Rayleigh number where the transition from the conduction to the convection regime occurs was found to be in the range of 7.869×10^6–3.237×10^7. It was found that the melt volume fraction and the time-averaged Nusselt number can be correlated by: $V/V_o = 4.73 Fo^{0.906}\ Ste^{1.538}\ Ra^{0.002}$ and $\overline{Nu} = 0.0219 Ra^{0.387}\ Pr^{0.0191} (H/\delta)^{0.0621}$ respectively. © 1999 Elsevier Science Ltd. All rights reserved.

1. Introduction

Heat transfer processes undergoing liquid–solid phase transformation have been of continuing interest for researchers. This is driven by the pool of applications that are associated with this phenomenon. A sample of applications include: freeze-drying of foodstuffs, growth of pure crystals, castings and latent-heat thermal energy storage systems. Better understanding of the mechanisms associated with phase change phenomenon facilitates maximizing the benefits of such a process. Part of this understanding in phase change problems requires information on predicting the instantaneous temperature distribution in both solid and liquid phases, tracing the liquid–solid interface and predicting the heat transfer across the heating surface.

In a rectangular enclosure with one of its vertical walls suddenly elevated to a higher temperature, a thin melt layer forms adjacent to the heated surface at the initial stage indicating that conduction is the dominant mode of heat transfer. As time progresses, the buoyancy induces a flow due to temperature gradient causing the melt volume at the top to recede at a faster rate compared to the bottom of the enclosure. The onset of natural convection causes the liquid–solid interface to curve, thus augmenting the melting process. Melting of pure substances in rectangular enclosures have received considerable attention. Viskanta [1] and Yao and Prusa [2] have documented the pertinent studies reported in the literature concerning phase change materials in enclosures. Considerable work has been devoted to the subject of pure substances undergoing a phase change process. Some approximate analytical solutions have also been presented [3,4].

* Corresponding author. Tel.: +1-614-292-6560; fax: +1-614-292-3163.

E-mail address: vafai.1@osu.edu (K. Vafai)

0017-9310/99/$ - see front matter © 1999 Elsevier Science Ltd. All rights reserved.
PII: S0017-9310(99)00024-1

Nomenclature

A_w	cross sectional area of the heating wall (m^2)
c	specific heat at constant pressure (J kg^{-1} K^{-1})
h	heat transfer coefficient (W m^{-2} K^{-1})
h_{sl}	latent heat (J kg^{-1})
Fo	Fourier number, $Fo=\alpha t/L^2$
H	height of the rectangular enclosure (m)
k	thermal conductivity (W m^{-1} K^{-1})
L	length of the rectangular enclosure (m)
n	time index
Nu	Nusselt number, hH/k_l
Pr	Prandtl number, v/α
Ra	Rayleigh number, $g\beta(T_w-T_m)H^3/\alpha v$
q_{loss}	heat loss to the ambient (W m^{-2})
q_w	wall heat flux (W m^{-2})
Q_{total}	total heat transfer (J)
$\dot{Q}$	instantaneous heat transfer (W)
Ste	Stefan number, $c(T_w-T_m)/h_{sl}$
t	time (s)
t_c	conduction time lag (s)
T	temperature (K)
V	volume (m^3)
V_o	volume of the enclosure (m^3)
X, Y	Cartesian coordinates of the melting front (m)

Greek symbols

α	thermal diffusivity (m^2 s^{-1})
β	thermal expansion coefficient (K^{-1})
δ	average interface location (m) defined in Eq. (9)
ν	kinematic viscosity (m^2 s^{-1})
ρ	density (kg m^{-3})

Subscripts

i	initial
l	liquid
m	melting point
s	solid
w	heat pipe wall

However, much of the emphasis has been on numerical simulations [5–9] of the process and to a lesser extent on developing an experimental data base. Some have also pursued a scaling analysis [10]. There exists a lack of sufficient experimental work in this regard. However, few exceptions do exist.

The series of experimental investigations conducted by Viskanta and co-workers [11–13] on a low-Prandtl number phase change material (PCM), namely gallium, have been widely considered for the purpose of comparison and benchmarking. The experimental results provided substantial physical insight into the general features of the phase change process and have constituted a classical benchmarking for numerical results. In these experiments, the heating source was provided by means of an isothermal wall temperature which remained fixed in time. A number of distinct features are associated with these experiments. Since gallium is identified as a liquid metal with a relatively small latent heat, the melting rate is quite fast. Moreover, the melting temperature is less than 30°C which makes it more prone to slight changes in ambient conditions. These factors make the precise prediction of temperature distribution and the instantaneous allocation of the liquid–solid interface a difficult task. In addition, imposing constant wall temperature was an approximation due to the finite capacity of the heat exchangers.

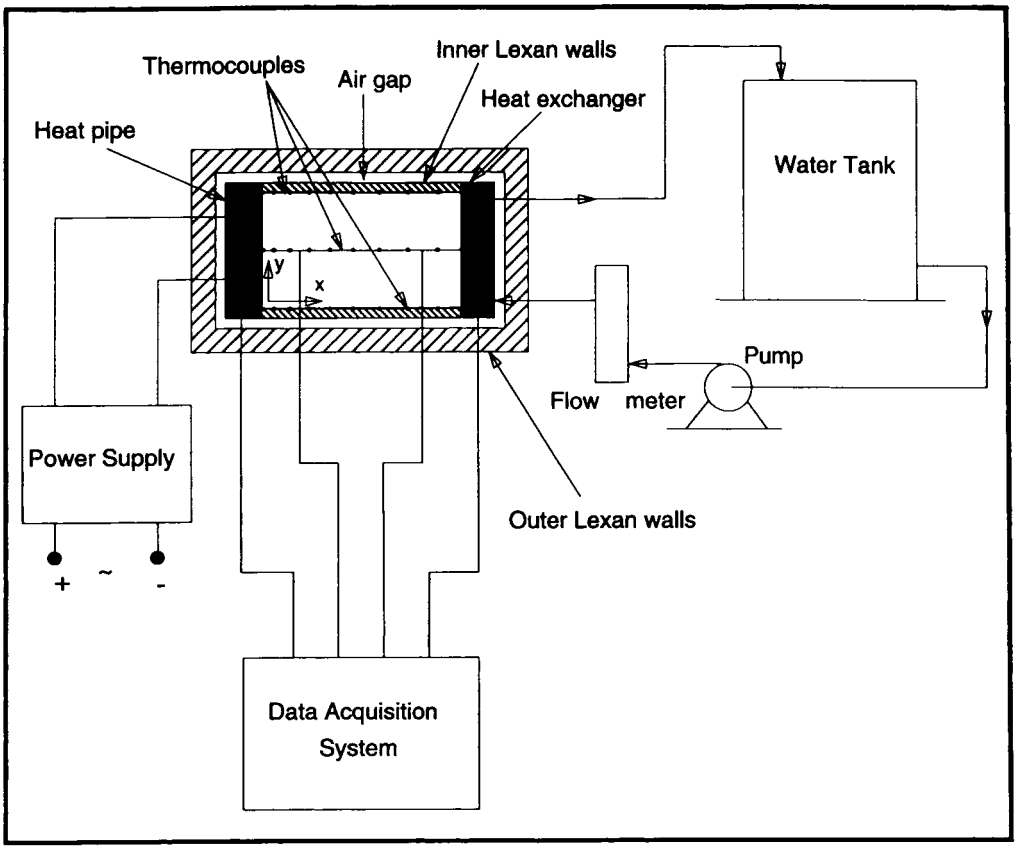

Fig. 1. Schematic diagram of the experimental apparatus.

Some of the aforementioned aspects as well as lack of sufficient experimental data base in this area sum up the motivation for undertaking the present investigation. The present experiment is based on direct visual measurement of the liquid–solid interface at all times, which was not done in earlier studies. Test runs were performed using a solid PCM with a high Prandtl number. It should be noted that such high Prandtl numbers have not been reported in the literature. In addition, in this experiment, the vertical heated wall was set up by means of a flat-plate heat pipe. The main advantage of the flat-plate heat pipe is the uniformity of temperature readings on the condenser side at any given time. This would provide a more accurate means of imposing the uniform wall temperature boundary condition which rises with time until steady state wall temperature is reached. As a result, the ongoing experiment could serve as a benchmarking tool for validating numerical results for PCM related applications.

The objective of the present experimental study is to provide more accurate means of tracing the temporal development of the liquid–solid interface through direct visual measurements and, also, to accurately measure the temperature distributions in the solid and the fluid domains. In addition, the contribution of the natural convection effect to the melting rate is demonstrated and examined. Furthermore, the critical Rayleigh number, where the transition from conduction to convection occurs, is identified for each test run. Finally, empirical correlations were developed, based on the experimental results, for the temporal melted volume fraction and the average Nusselt number at any given time as a function of the pertinent dimensionless groups. In what follows, the experimental apparatus and procedure will be described first, whereafter the results will be discussed.

2. Experimental apparatus and procedures

A schematic diagram of the apparatus employed in this study is shown in Fig. 1. The setup is designed to provide accurate measurements of the instantaneous interface and temperature distributions. The setup allows for multiple and repetitive experiments.

Transparent materials were utilized whenever possible to enhance visualization. The test cell is made up of an enclosure of a rectangular cross section with inside dimensions of 153 mm in width, 103 mm in height and 103 mm in depth. The top, bottom, front and back walls were made of Lexan with a plate thickness of 12.2 mm. The assembled unit was housed in a second container made of Lexan to minimize the heat loss to the environment. A dead air gap of 12.7 mm was maintained between the assembled unit and the container on all sides. Lexan has a low thermal conductivity ($k = 0.2\ \mathrm{W\ m^{-1}\ K^{-1}}$). This low thermal conductivity along with the air gap substantially reduce the heat losses. A feed line was connected to a hole on the top plate to compensate for any change in volume during the phase change process. The two vertical side walls served as the heat source and sink. A flat plate heat pipe (103×103 mm) was attached to the left side of the enclosure facing the PCM as shown in Fig. 1. The heat pipe walls were made out of copper. Also, the heat pipe was heated via a very thin heater strip (103×25.4 mm) attached to its back. The condenser surfaces of the heat pipe on the same side as the heating strip were insulated to reduce heat losses. The heat sink constituted of a heat exchanger attached to the right side of the enclosure. The heat exchanger was fabricated using copper plates along with two baffles welded to one plate to ensure good mixing of the cooling water and, thus, enhancing the heat transfer coefficient. The water flow was circulated through a constant-temperature relatively large water tank, and the flow rate was regulated by a flow meter. Substantial measures were taken to eliminate any leakage from the assembled unit (enclosure, heat pipe and heat exchanger) during the phase change process. Thin layers of gasket were placed between the different parts during the assembly process.

Polyethylene glycol 900 (PEG900) was used as the phase change material for the current investigation. The properties of this PCM are given below:

Liquid phase	Solid phase
$\rho = 1100\ \mathrm{kg\ m^{-3}}$	$\rho = 1120\ \mathrm{kg\ m^{-3}}$
$c = 2260\ \mathrm{J\ kg^{-1}\ K^{-1}}$	$c = 2260\ \mathrm{J\ kg^{-1}\ K^{-1}}$
$k = 0.188\ \mathrm{W\ m^{-1}\ K^{-1}}$	$k = 0.188\ \mathrm{W\ m^{-1}\ K^{-1}}$

$$\beta = 7.6 \times 10^{-4}\ \mathrm{K} \quad h_{\mathrm{sl}} = 150.5\ \mathrm{kJ\ kg^{-1}} \quad T_{\mathrm{m}} = 34^{\circ}\mathrm{C}$$

This particular PCM has several advantages and it appears that it has not been utilized before in the literature. It has both a moderate melting point as well as heat of fusion. These features expand the duration of an experiment, as compared to gallium as the PCM, thus allowing better visualizing and monitoring of the melting process. Additional thermophysical properties are listed in Table 1.

Table 1
Thermophysical properties of PEG900

Temperature (°C)	ν ($\mathrm{m^2\ s^{-1}}$)	Pr
32.2	9.0	1188
51.7	5.4	713
65.6	3.4	449

The surface temperature of the heat pipe and that of the heat exchanger were each measured by six E-type thermocouples. The thermocouples were placed in a shallow rectangular groove especially fabricated on each surface and were then firmly glued to the surface facing the PCM. The heat pipe surface temperature facing the PCM was found to be spatially uniform throughout the cycle of a test run, while the spatial temperature variation on the heat exchanger surface was found to be very small. The heat exchanger surface temperature was computed by averaging the six thermocouples' readings. The discrepancies in heat exchanger temperature was maintained to within $\pm 0.2^{\circ}\mathrm{C}$ by adjusting its pumping power during the course of the phase change process. Throughout the experiments, the temperature readings were taken at the central region of the corresponding surface in order to retain the two-dimensional behavior of the enclosure and to minimize the end effects. The temperature distributions along the mid-plane, top and bottom walls were measured using thermocouples which were variably spaced. The thermocouples were closer in space near the heat pipe and were further distanced as approaching the heat exchanger. This would allow more accurate calculation of the convective heat transfer rate near the wall in terms of the dimensionless variable, namely the Nusselt number and the shape of the melting front. The exact positions of the thermocouples were prescribed at 4.7, 14.7, 30.0, 45.3, 60.6, 75.9, 91.2, 106.5, 121.8, 137.1 and 153.2 mm from the heat pipe wall. The thermocouples were placed in small stainless steel tubes (1.6 mm diameter) which were drilled in the plates such that the desired positions were maintained. All thermocouples were sealed and their ends were coated with a thin layer of a high-temperature cement for protection and improvement of the measurements.

Twenty E-type thermocouples (10 in each plate) were placed at the top and the bottom plates. The thermocouples' ends were carefully placed at the inner surface of the plates such that close contact with the PCM is achieved. For each of the upper and lower plates, and the mid-plane, the temperature distribution was measured in a direction perpendicular to the hot

Table 2
The input heat flux and the time lag values for the five case studies

Case	q_w (W m^{-2})	t_c (h)
1	2307	2.034
2	3945	0.564
3	5625	0.469
4	7075	0.424
5	9012	0.287

and cold vertical walls. The thermocouples were placed in stainless steel sleeves and inserted into the drilled wells on the frontal plate. The location of the thermocouples' junctions were ensured to within ± 0.5 mm from the surface of the heat pipe surface as well as the bottom of the enclosure. The sleeves were then passed through the holes to a central region and were firmly held at their ends. This particular design ensures that the thermocouples' junctions would remain at their original prescribed places when the liquid–solid interface passes through them. The heat loss from the phase change material to the surroundings was found to be very small. The interface location was measured every 30 min. A Data Acquisition system was used to record all the temperature readings. The power supply was turned off after the desired melted volume was obtained. The heating period was anywhere from 4 to 12 h depending on the power supply for each test run.

The uncertainty of the location of the liquid–solid interface was estimated to be ± 0.5 mm. Based on the uncertainty analysis method of Kline and McClintock [14], the maximum uncertainties are $\pm 13.9\%$ for melted volume, $\pm 7.1\%$ for calculated heat transfer from the heat pipe surface to the PCM, and $\pm 7.3\%$ for both heat transfer coefficient, h, and Nusselt number, Nu.

3. Results and discussion

In this section, the principal results during the course of this investigation are documented. Five different test runs were performed by varying the input power to the heat pipe. Since the experimental data are sought to serve as a benchmark for validating future work, the input heat flux was used as a base for evaluating different cases. Table 2 lists the heat flux q_w for different cases. The focus will now be shifted to the presentation of the results and to the observations and conclusions that can be deduced from them.

The five case studies performed are demonstrated in Fig. 2 in terms of the temporal fractions of the melted volume. It can be seen that the melted volume fraction is a linear function of time except at the very beginning when conduction mode is the dominant mode of heat transfer. This linear relation can be expressed as follows

$$V/V_o = b(t - t_c) \tag{1}$$

where V is the volume of the melt, V_o is the volume of the enclosure and t is the elapsed time in hours. The time lag t_c accounts for the duration of the initial con-

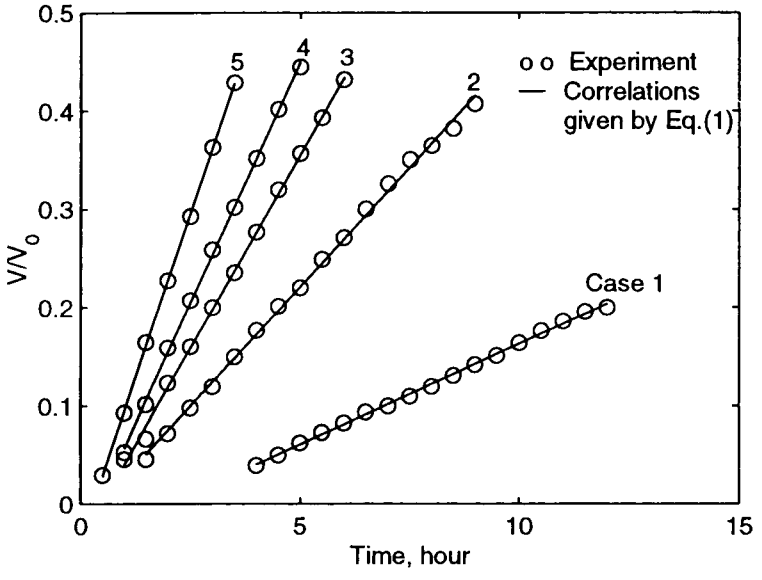

Fig. 2. Temporal fractions of the melted volume of the PCM for cases 1–5.

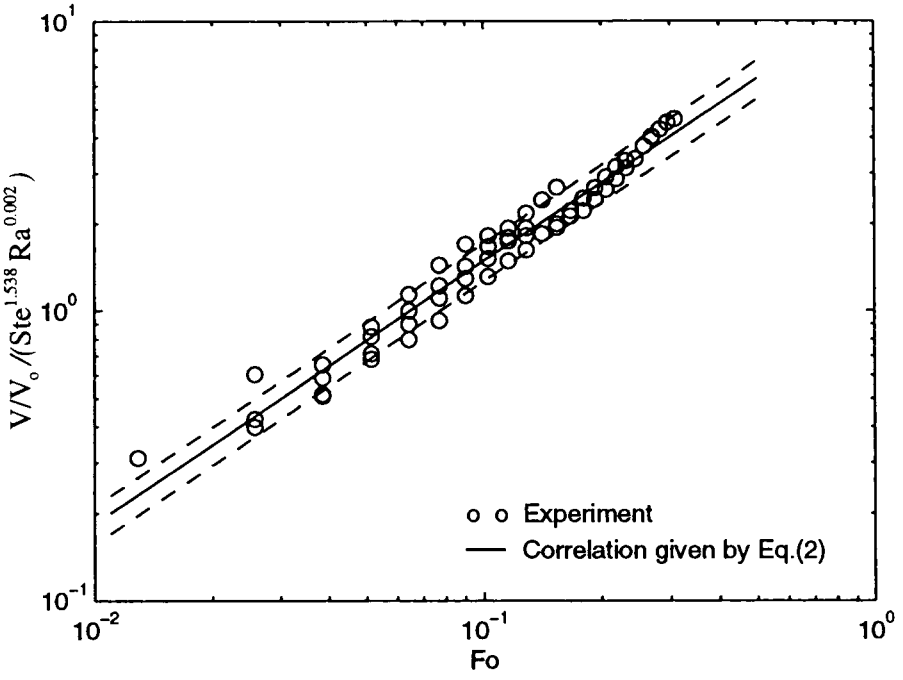

Fig. 3. Correlation for the fraction of the melted volume.

duction regime. The numerical value of t_c for the different cases is documented in Table 2. The fraction of the melted volume V/V_o was found to be proportional to $Fo^{0.906}$, where Fo is the Fourier number. The experimental data for the melted volume fractions for the entire duration of test runs were presented in terms of Fo, Rayleigh number Ra and Stefan number Ste. The data were generated from the five case studies and were found to be well correlated by the following dimensionless form

$$V/V_o = 4.73 Fo^{0.906}\, Ste^{1.538}\, Ra^{0.002}. \quad (2)$$

The dependency of the correlation on the Rayleigh number was found to be minimal. The experimental data and the correlation presented by Eq. (2) are displayed in Fig. 3. The empirical correlation predicts the experimental data with an average error of 9.3%. Much of the deviation of the experimental data is apparently caused by the sensible heating that takes place at the very early times due to the presence of the subcooling within the PCM. The dimensionless groups Fo and Ste are the most essential factors in controlling the melted volume. The results obtained by Gau and Viskanta [12] shows that V/V_o is proportional to $Fo^{0.842}\, Ste^{0.881}$. The exponents for Fo seem to be in good agreement. However, the exponent for Ste obtained in this investigation is almost twice as large as that reported in Gau and Viskanta [12]. The discrepancies may be attributed to the different thermophysical properties and to the much faster melting process attained by gallium. In addition, the current investigation covers a wider range of Fo (0.013–0.309) and Ste (0.081–0.405) which can reduce the creeping of errors when an empirical correlation is sought.

Fig. 4 illustrates the instantaneous marching of the liquid–solid interface in the axial direction, measured at prescribed normal positions. The interface locations are measured at prescribed normal positions at 0, 20, 40, 50, 60, 70, 80, 90, 103 mm from the bottom wall. For a given case study, the results show that the melting front is not a function of the normal coordinate at early times after activating the heat source. This is due to subcooling of PCM and conduction being the dominant mode of heat transfer in the initial stage resulting in the formation of a thin layer of melt parallel to the constant temperature condensation surface of the heat pipe. Once past the initial stage, buoyancy effect in the melt becomes more significant, causing faster transformation of the solid phase into liquid. Furthermore, the interface axial position increases almost linearly with time at any given normal location, after the conduction dominated regime. As expected, the advancement rate of the interface depends on the input heat flux. Fig. 5 depicts the history of the liquid–solid interface and clearly captures the development of the distinct shape of the melting front. In this figure, X and Y represent the horizontal and vertical coordinates of

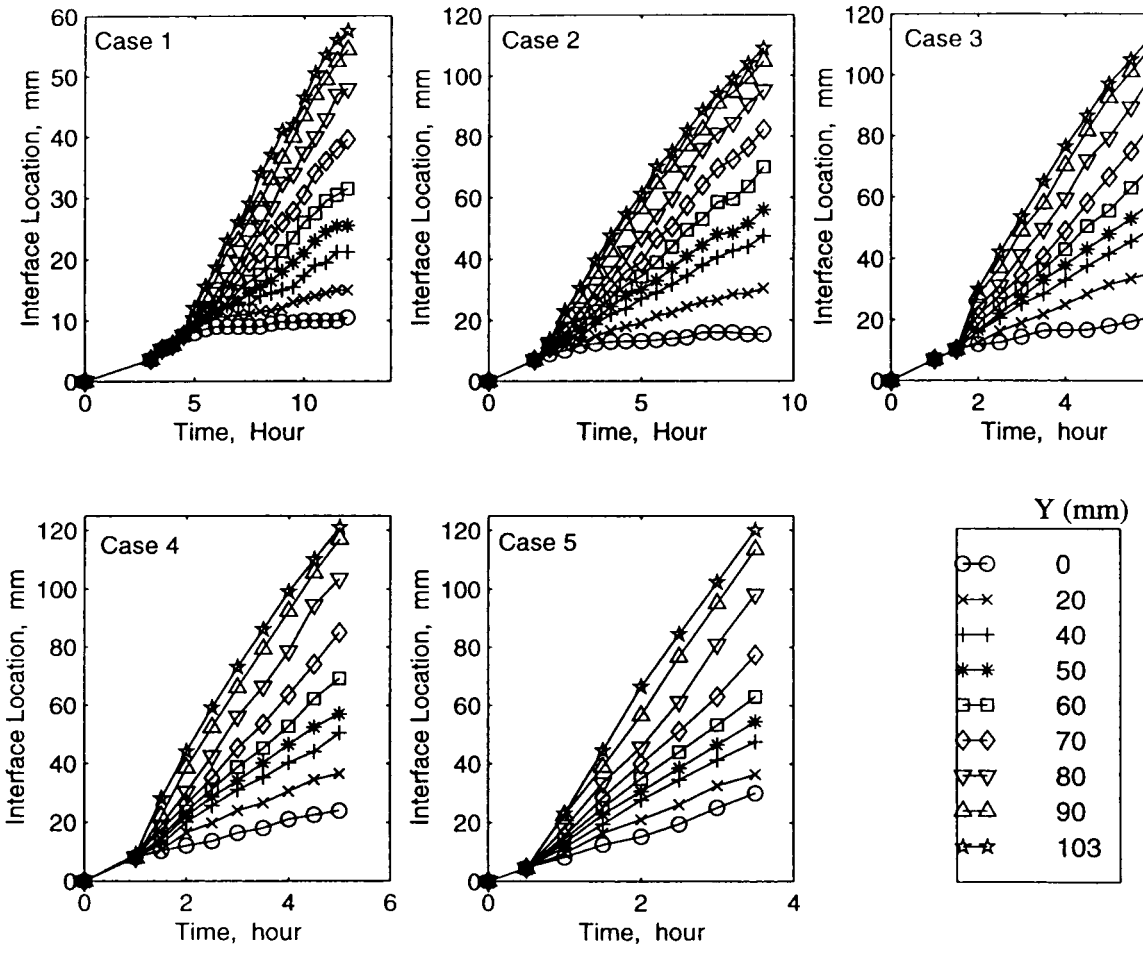

Fig. 4. Liquid–solid interface advancement in the axial direction at various normal positions.

the melting front. The results document the initial conduction regime and the onset of natural convection at later times. As expected, the increase in heat transfer activities due to the presence of natural convection results in larger melt volume at the top of the enclosure and the difference in the melting rate between the top and bottom walls causes the interface shape to curve as displayed in Fig. 5. Again, faster marching of the melting front was achieved by an increase in the supplied heat flux. Similar liquid–solid interface configurations were also reported by earlier numerical [6–10] and experimental studies [12,13].

Temporal temperature variations of the heat pipe and the heat exchanger surfaces are plotted against time for different values of heat flux input as shown in Fig. 6. As stated earlier, the heat pipe maintains a uniform temperature at any time over the condenser surface facing the PCM and it finally achieves a steady state value. In addition, the duration of the transient stage and the magnitude of the steady state temperature depend on the input heat flux. It can also be seen from Fig. 6 that the heat exchanger temperature remains constant for the duration of any given experiment. The initial temperature of the system and the final wall temperature for different cases are given in Table 3. Also, the temporal wall temperature history is given in Table 4 for different cases. The temperature distributions at the top and the bottom walls as well as in the mid-plane are shown in Figs. 7 and 8. The presentation of the data are limited to cases 1 and 3 only

Table 3
Initial temperature of the system and the final wall temperature

Case	1	2	3	4	5
Initial temperature	20.93	22.56	21.38	21.20	23.12
Final wall temperature	42.42	50.98	53.80	58.96	60.61

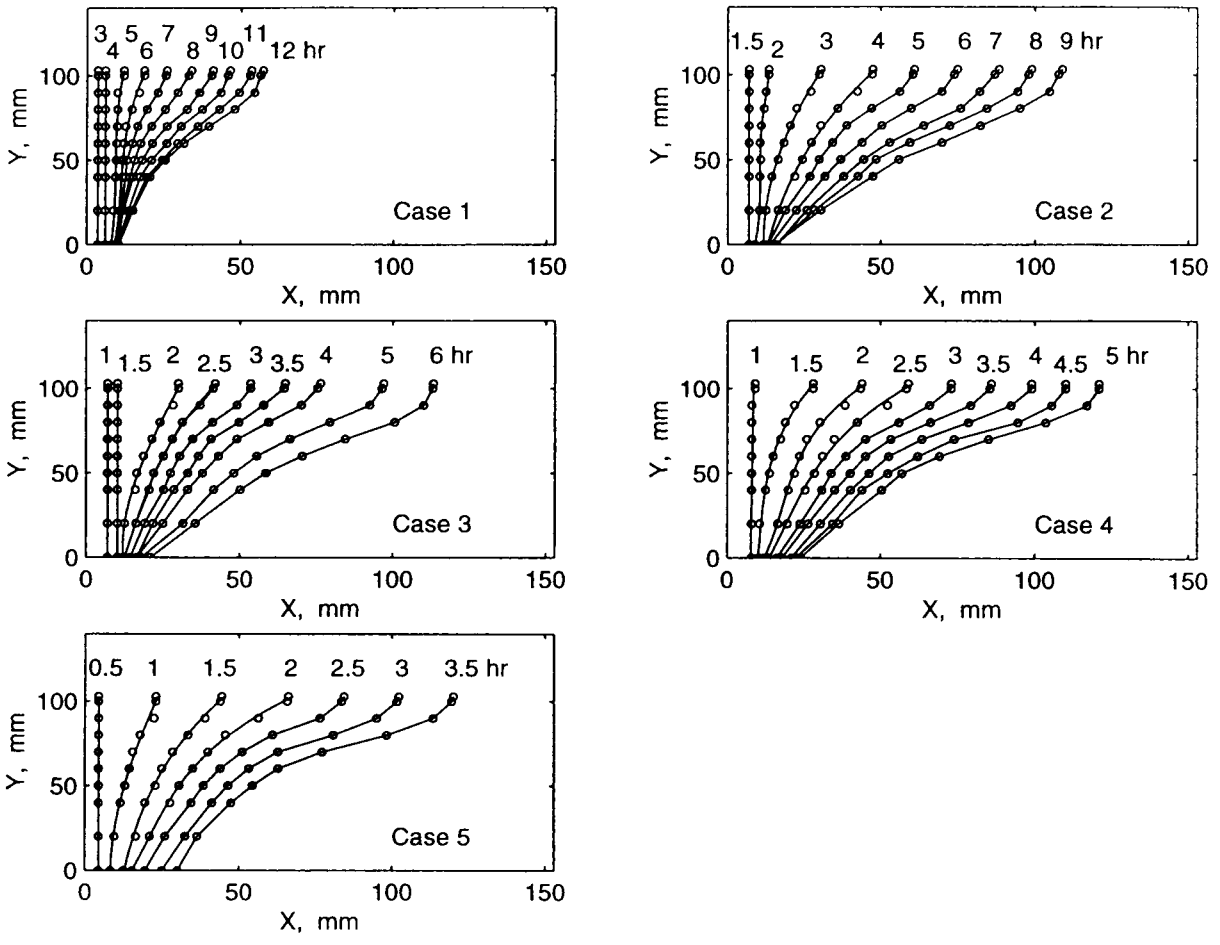

Fig. 5. Temporal evolution of the liquid–solid interface.

since all the considered cases were found to exhibit similar patterns of thermal behavior. As expected, the temperature readings at the very early times were about the same for all three planes. The temperature variation at the top wall exhibited similar distribution to that at the bottom wall until the heat pipe reached its maximum temperature, i.e. steady-state condition. Thereafter, the thermal boundary layer near the liquid–solid interface constituted a large portion of the total thermal resistance. The recorded temperature values were found to be the highest at the top wall and the lowest at the bottom wall as time progressed due to the onset of the buoyancy-driven flow. The increase in flow circulation in the melt region near the heat pipe enhances the heat transfer from the heating wall. It was observed that the temperature at the top wall

Table 4
Wall temperature history: $T_w = At^5 + Bt^4 + Ct^3 + Dt^2 + Et + F$, where t is given in min

Case	1	2	3	4	5
A	1.35×10^{-12}	9.70×10^{-12}	5.02×10^{-11}	1.20×10^{-10}	5.13×10^{-10}
B	-2.62×10^{-9}	-1.59×10^{-8}	-5.84×10^{-8}	-1.18×10^{-7}	-3.80×10^{-7}
C	1.94×10^{-6}	1.00×10^{-5}	2.67×10^{-5}	4.60×10^{-5}	1.12×10^{-4}
D	-7.36×10^{-4}	-3.06×10^{-3}	-6.02×10^{-3}	-8.98×10^{-3}	-1.67×10^{-2}
E	0.167	0.460	0.684	0.897	1.25
F	22.6	23.9	22.4	22.2	23.5

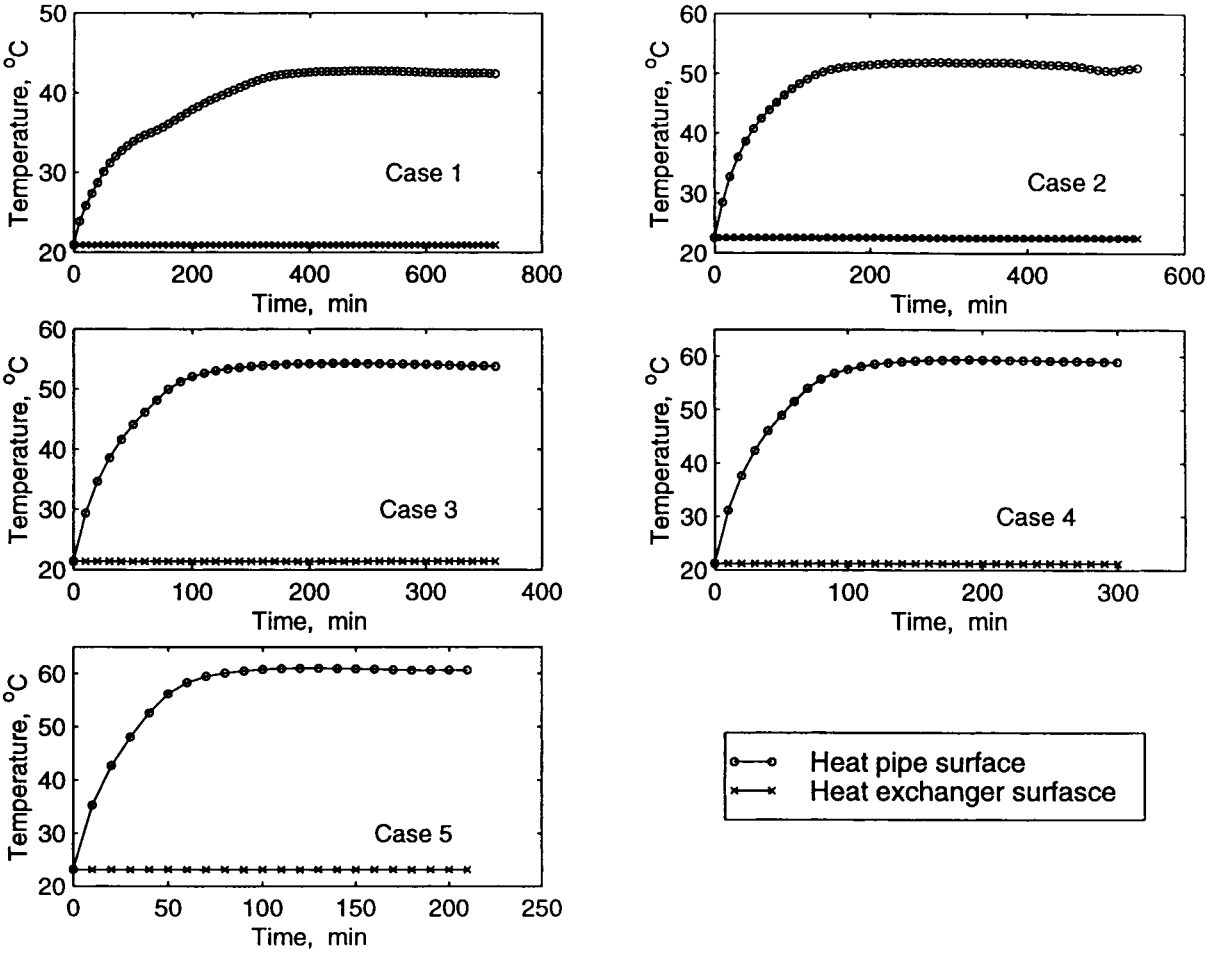

Fig. 6. Transient heat pipe and heat exchanger surface temperature distributions.

decreased almost linearly with the location away from the heating wall except in the vicinity of the interface, where the temperature decreased sharply. Moreover, the near-wall temperature decreased most sharply at the bottom region, while it was least sharp at the top region.

As can be seen in Figs. 7 and 8, for longer times the mid-plane temperature in the melted domain was quite uniform except in the vicinity of the heat pipe and the interface. This was especially the case for higher heat inputs. The thermal resistance in the core region could be neglected due to relatively stronger convection. This is true for a PCM with a large Prandtl number where the thermal boundary layer is confined to within a close distance from the heating wall. In view of these results, one can deduce that the heat transfer regime in the top and the mid-plane parts are dominated by natural convection while the bottom part is conduction dominated. This is in accordance with the observations documented earlier regarding the curved interface shape.

The Nusselt number on the heated wall is a function of the total heat input to the PCM. The heat transferred to the PCM, Q, can be computed as follows:

$$Q = \rho_l V_l h_{sl} + \int_{V_i(t)} \rho_s c_s (T_m - T_i)\, dV_l + \int_{V_i(t)} \rho_l c_l (T_l - T_m)\, dV_l + \int_{V_s(t)} \rho_s c_s (T_s - T_i)\, dV_s + \int_t q_{loss}\, dt \quad (3)$$

In the above equation, the first term on the right hand side accounts for the latent heat of fusion that is absorbed by the PCM during the phase transformation. The next two integral quantities represent the temperature rise in the solid PCM to its melting point

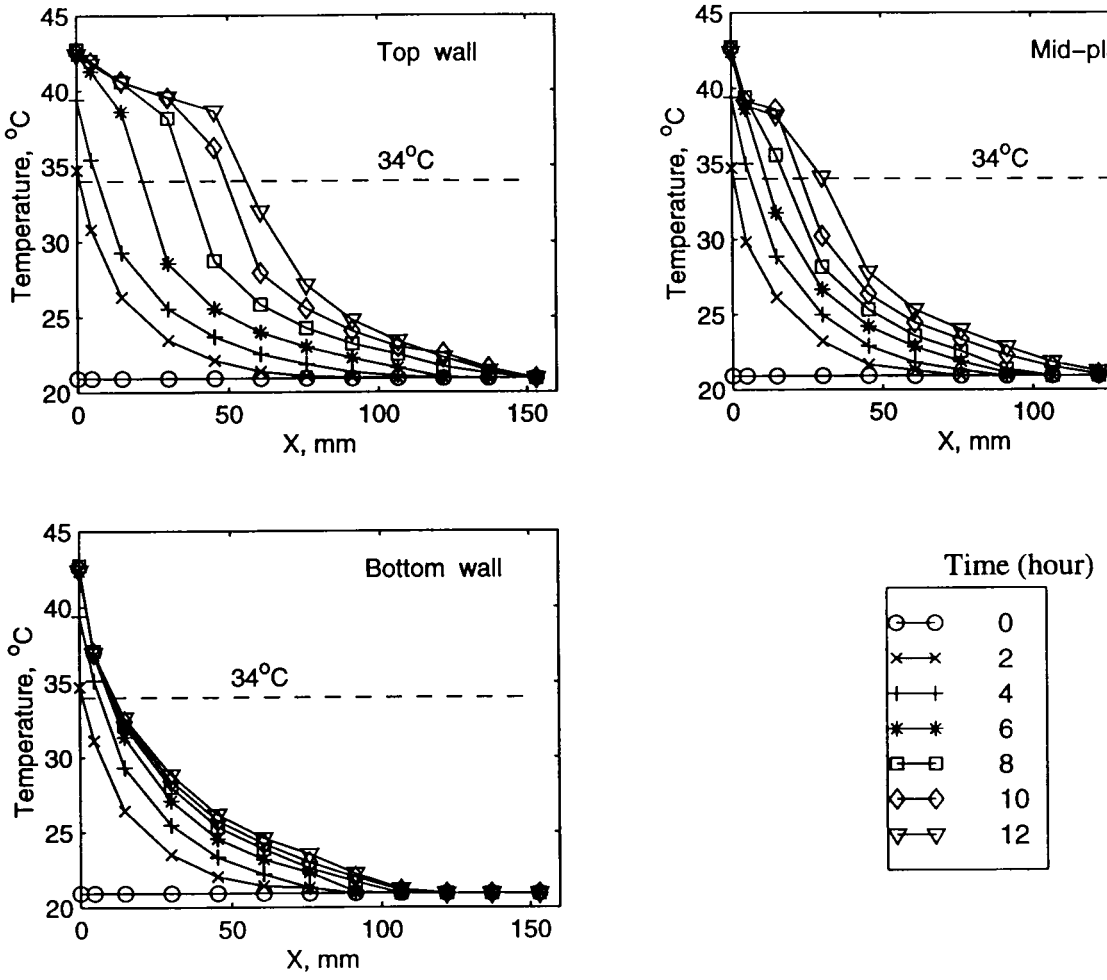

Fig. 7. Temperature distributions along the top, mid-plane and bottom walls for case 1.

and in superheating of the liquid phase respectively. In addition, the third integral accounts for the sensible heating of the solid phase. The heat loss due to the ambient, q_{loss}, was found to be very small. A closer look at the temperature distribution in Figs. 7 and 8 show that the temperature gradient approaches zero at the heat exchanger side. This observation is especially true at the bottom wall where heat transfer is negligible. The low thermal conductivity of the PCM and the good insulation provided for the enclosure aid in this regard. The temporal heat transfer coefficient can be obtained from

$$h = \frac{\dot{Q}}{A_w(T_w - T_m)} \tag{4}$$

where Q is the instantaneous heat transfer and A_w is the cross sectional area of the heating wall. In a similar manner, the average heat transfer coefficient is given by

$$\bar{h} = \frac{Q_{total}}{A_w(T_w - T_m)t_n} \tag{5}$$

where Q_{total} is the total heat transfer to the PCM from the start of a test run and t_n is the corresponding elapsed time. Finally the temporal Nusselt number can be expressed in the conventional fashion as:

$$Nu = \frac{hH}{k_l} \tag{6}$$

and the time-average Nusselt number as

$$\overline{Nu} = \frac{\bar{h}H}{k_l} \tag{7}$$

The characteristic length was taken to be the height of the enclosure since the melting front position is vari-

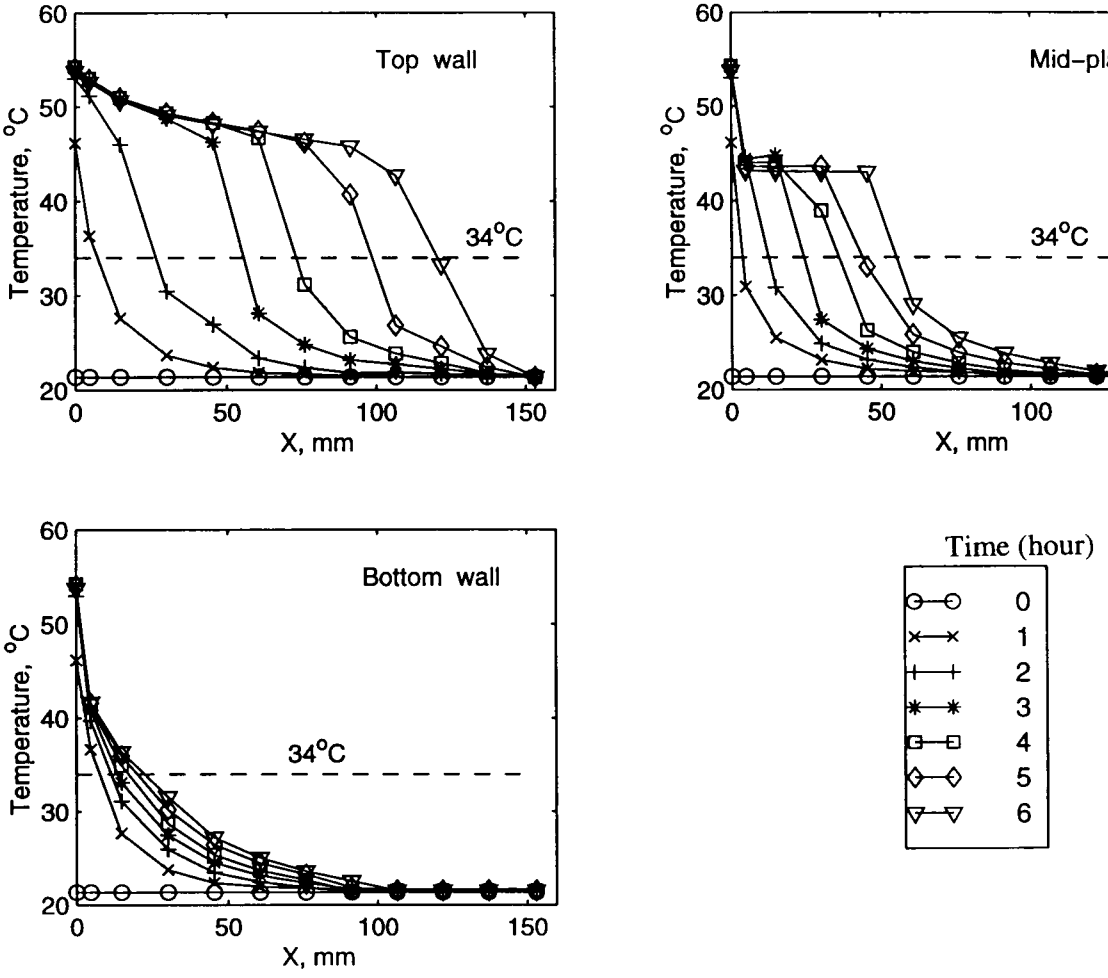

Fig. 8. Temperature distributions along the top, mid-plane and bottom walls for case 3.

able. The temporal and the average Nusselt number results are shown in Fig. 9. The natural convection flow was laminar for the duration of the melting process. The temporal Nusselt number reflects the presence of three different regimes during the melting process. The first regime is the conduction regime which appears at the beginning of the melting process and is characterized by the relatively large magnitude of the Nusselt number that decreases as time elapses. The large Nusselt number results are attributed to the minimal heat losses to surroundings at the early times, thus, giving rise to the total heat transferred to a thin layer of melt. In addition, the temperature difference $(T_w - T_m)$ is quite small at the startup time which accordingly increases the magnitude of the Nusselt number. The second regime is the convection regime, where natural convection dominates the heat transfer process. The convection aids in increasing the Nusselt number, but the Nusselt number eventually decays to an asymptotic value due to the increase in the thickness of the melting layer. Between these two regimes lies the transition regime where both conduction and convection are prime factors in the heat transfer process. However, natural convection becomes more significant as time progresses. This phenomena has also been observed by an earlier study [13].

The transitional or critical Rayleigh number, Ra_{cr}, is defined as the Rayleigh number where the transition from the conduction to the convection regime does occur. The critical Rayleigh number for each case was determined by identifying the time when the temporal Nusselt number recovers from its first minima. Another evidence of transition is depicted in the slight drop in the heat pipe surface temperature. The Ra_{cr} for cases 1–5 were found to be 6.41×10^6, 2.61×10^7, 2.20×10^7, 2.97×10^6 and 2.02×10^6 respectively, and

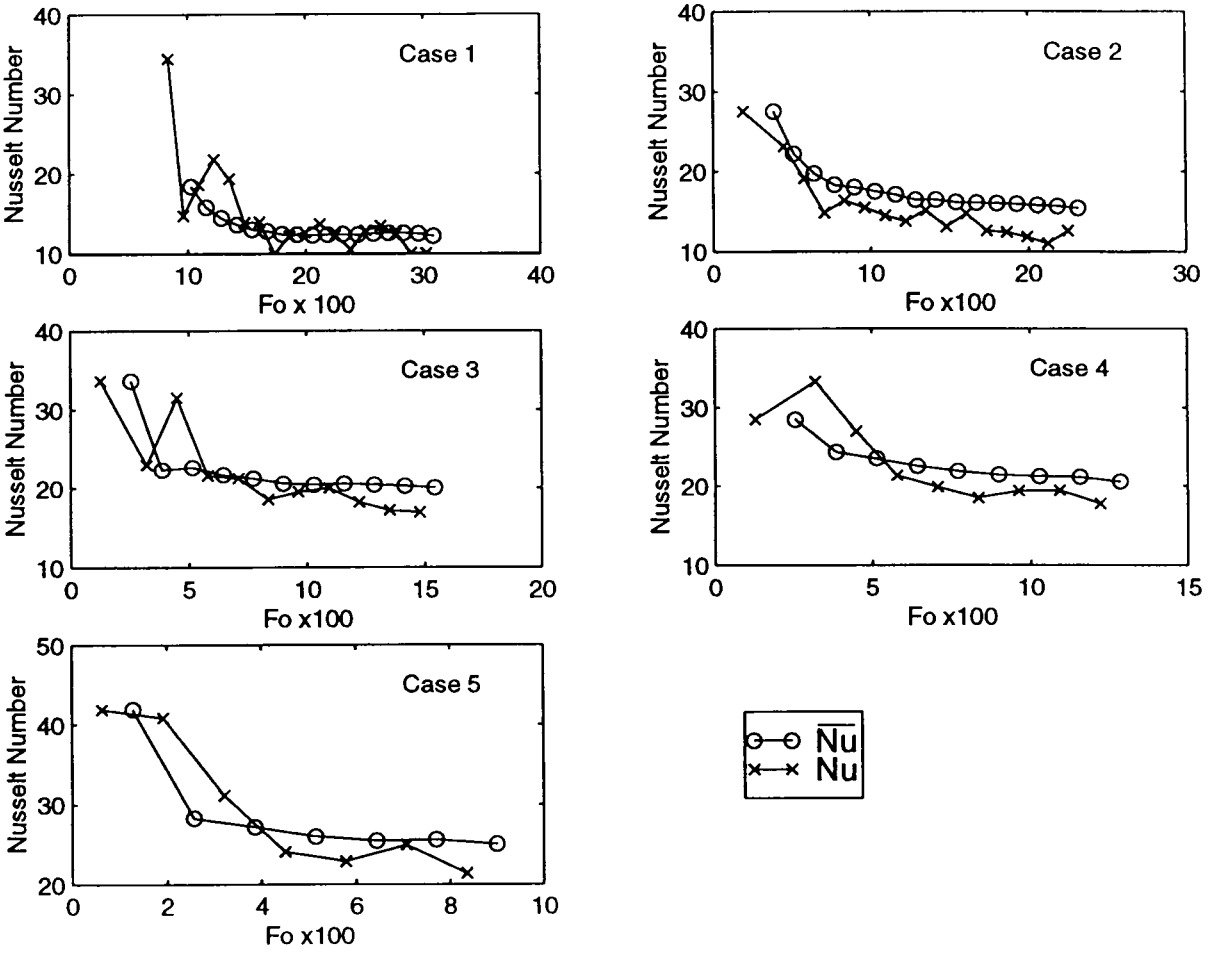

Fig. 9. Temporal and time-averaged Nusselt numbers variations.

are in agreement with the changes of the interface configurations. This finding is of significance in predicting the development of the interface shape. It is apparent that for all the cases the average Nusselt number shares the tendency to monotomically decrease with time. In addition, the results indicate that substantial drop in the Nusselt number occurs while the initial conduction regime is passed. This is due to the growth of the thermal boundary layer which lowers the capability of carrying out the energy from the heated wall. The following correlation reduces the average Nusselt number for the individual five cases in Fig. 9 to a single equation

$$\overline{Nu} = 0.0219 Ra^{0.387}\, Pr^{0.019} (H/\delta)^{0.062} \tag{8}$$

where δ is the average interface location which is given by

$$\delta = \frac{\int_0^H X \,\mathrm{d}y}{H} \tag{9}$$

where X is the axial coordinate of the melting front. The choice of (H/δ) is more suitable than (H/L) since it considers the development of the melting front as time progresses. The correlation represents the time-averaged Nusselt number for the entire melting process and it covers the following range of dimensionless groups: $Ra = 8.56 \times 10^6$–4.78×10^7, $Pr = 804 - 1055$ and $(H/\delta) = 1.5$–13.6. Eq. (8) was found to fit the data for the individual five cases with an average error of 8.8%. Fig. 10 compares the average Nusselt numbers obtained from Eq. (8) against the experimental data. As shown in Fig. 10, this general correlation collapses the data fairly well. Furthermore, the value of the Rayleigh number is shown to be the main dimensionless group in affecting the Nusselt number results. Table 5 lists the exponent value of the Rayleigh num-

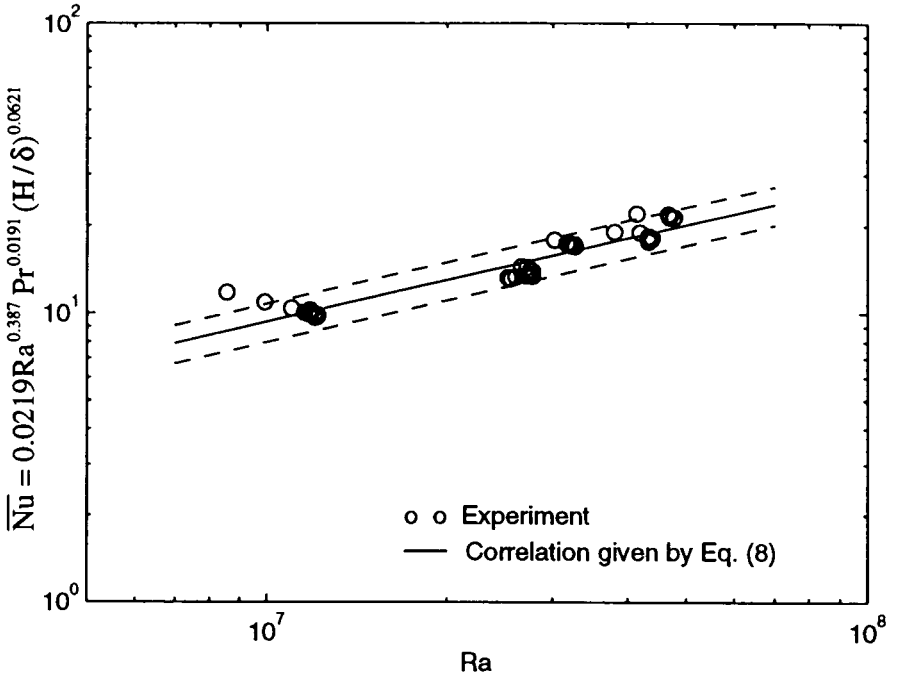

Fig. 10. Correlation of the time-average Nusselt number.

ber for some of the related works in the literature. The difference in the exponent is attributed to the variation in the thermophysical properties and the wider range of applicability for the present correlation. Again, it should be emphasized that the Prandtl number ratio between the current investigation and the rest of the documented studies in Table 5 is of the order of 10^5.

4. Conclusions

In this work, an experimental investigation was conducted to examine the thermal characteristics of the melting process in a rectangular enclosure heated from a vertical side. A flat plate heat pipe was utilized to provide a uniform temperature wall at any given time. A high Prandtl number material was considered for this investigation which has not been reported on before. The presentation of the results clearly captures the development of the distinct structure of the liquid–solid interface in the presence of natural convection. The temperature distributions in the PCM along the top wall, mid-plane and the bottom wall were presented. It was shown that the temporal Nusselt number results distinguishes three different heat transfer regimes during the melting process. Correlations, developed for the melted volume fraction and the time-averaged Nusselt number as a function of the parametric variables, were found to yield good agreement with the experimental data. The detailed data and correlations given in the present work address a needed gap resulting from a lack of sufficient experimental data in this area.

Table 5
The exponent of Rayleigh number which appears in the time-averaged Nusselt number, Eq. (8)

Studies	n
Webb and Viskanta [5]	0.263
Gau and Viskanta [12]	0.274
Beckermann and Viskanta [13]	0.250
Current investigation	0.387

References

[1] R. Viskanta, Heat transfer during melting and solidification of metals, J. Heat Transfer 110 (1988) 1205–1219.
[2] L.S. Yao, J. Prusa, Melting and freezing, Adv. Heat Transfer 19 (1989) 1–95.
[3] E.M. Sparrow, S.V. Patankar, S. Ramadhyani, Analysis of melting in the presence of natural convection in the melt region, J. Heat Transfer 99 (1977) 520–526.
[4] M. Okada, Analysis of heat transfer during melting

from a vertical wall, Int. J. Heat Mass Transfer 27 (1984) 2057–2066.
[5] B.W. Webb, R. Viskanta, Analysis of heat transfer during melting of a pure metal from an isothermal vertical wall, Numerical Heat Transfer 9 (1986) 539–558.
[6] A.D. Brent, V.R. Voller, K.J. Reid, Enthalpy–porosity technique for modelling convection–diffusion phase change: application to the melting of a pure metal, Numerical Heat Transfer 13 (1988) 297–318.
[7] M. Lacroix, V.R. Voller, Finite difference solutions of solidification phase change problems: transformed versus fixed grids, Numerical Heat Transfer, Part B 17 (1990) 25–41.
[8] C.P. Desai, K. Vafai, A unified examination of the melting process within a two-dimensional rectangular cavity, J. Heat Transfer 115 (1993) 1072–1075.
[9] S.C. Huang, Analytical solution for the buoyancy flow during the melting of vertical semi-infinite region, Int. J. Heat Mass Transfer 28 (1985) 1231.
[10] P. Jany, A. Bejan, Scaling theory of melting with natural convection in enclosures, Int. J. Heat Mass Transfer 31 (1988) 1221–1235.
[11] C. Gau, R. Viskanta, Melting and solidification of a metal system in a rectangular cavity, Int. J. Heat Transfer 27 (1984) 113–123.
[12] C. Gau, R. Viskanta, Melting and solidification of a pure metal on a vertical wall, J. Heat Transfer 108 (1986) 174–181.
[13] C. Beckermann, R. Viskanta, Effect of solid subcooling on natural convection melting of a pure metal, J. Heat Transfer 11 (1989) 416–424.
[14] S.J. Kline, F.A. McClintock, Describing uncertainties in single sample experiments, Mechanical Engineering 75 (1) (1953) 3–8.